ADVANCED MATERIALS

slowly added to the mixture, which was stirred for 1.5 h at 85 °C in the dark. The reaction mixture was then poured into 2.5 L of methanol containing 20 mL of hydrochloric acid and 20 mL of hypophosphorous acid (H_3PO_2). The precipitate was isolated by centrifugation (3500 rpm, 5 min) and dissolved into a small amount of chloroform. The prepolymer solution was spin-coated as follows: Prepolymer (5 mg) was dissolved in 2 mL of chloroform, and the solution was dropped onto a quartz or CaF_2 plate. The plate was then rotated at 1200 rpm for 30 s. A thin film of poly(**1b**)-c formed after evaporation of the solvent (at room temperature).

Received: October 29, 2002
Final version: February 1, 2003

[1] H. Duerr, H. Bouas-Laurent, *Photochromism: Molecules and Systems*, Studies in Organic Chemistry, Vol. 40, Elsevier, Amsterdam **1990**.
[2] a) M. Irie, *Chem. Rev.* **2000**, *100*, 1685. b) M. Irie, M. Mohri, *J. Org. Chem.* **1988**, *53*, 803. c) M. Irie, K. Uchida, *Bull. Chem. Soc. Jpn.* **1998**, *73*, 985. d) S. H. Kawai, S. L. Gilat, J.-M. Lehn, *Chem. Eur. J.* **1995**, *1*, 285. e) G. M. Tsivgoulis, J.-M. Lehn, *Chem. Eur. J.* **1996**, *2*, 1399.
[3] a) N. Tanio, M. Irie, *Jpn. J. Appl. Phys.* **1994**, *33*, 1914. b) T. Tsujioka, F. Tatezono, T. Harada, K. Kuroki, M. Irie, *Jpn. J. Appl. Phys.* **1994**, *33*, 5788.
[4] a) S. Kobatake, K. Shibata, K. Uchida, M. Irie, *J. Am. Chem. Soc.* **2000**, *122*, 12 135. b) M. Irie, T. Lifka, S. Kobatake, N. Kato, *J. Am. Chem. Soc.* **2000**, *122*, 4871. c) T. Yamada, S. Kobatake, K. Muto, M. Irie, *J. Am. Chem. Soc.* **2000**, *122*, 1589. d) M. Irie, K. Uchida, T. Eriguchi, H. Tsuzuki, *Chem. Lett.* **1995**, 899.
[5] F. Stellacci, C. Bertarelli, F. Toscano, M. C. Gallazzi, G. Zerbi, *Chem. Phys. Lett.* **1999**, *302*, 563.
[6] J. H. G. Steinke, I. R. Dunkin, D. C. Sherrington, *Macromolecules* **1996**, *29*, 407.
[7] M. Irie, K. Sakemura, M. Okinaka, K. Uchida, *J. Org. Chem.* **1995**, *60*, 8305.
[8] K. Matsuda, M. Irie, *Chem. Eur. J.* **2001**, *7*, 3466.
[9] a) Y. Yokoyama, Y. Kurita, *Nippon Kagaku Kaishi* **1992**, 998. b) Y. Yokoyama, Y. Kurita, *Synth. Org. Chem. Jpn.* **1991**, *49*, 364.
[10] A. S. Hay, *Polym. Eng. Sci.* **1976**, *16*, 1.
[11] K. Uchida, A. Takata, S. Nakamura, M. Irie, *Chem. Lett.* **2002**, 476.
[12] The irradiation time could be reduced to less than 100 ms by focusing the light into a small spot.
[13] T. Kaieda, S. Kobatake, H. Miyasaka, M. Murakami, N. Iwai, Y. Nagata, A. Itaya, M. Irie, *J. Am. Chem. Soc.* **2002**, *124*, 2015.
[14] K. Uchida, M. Saito, A. Murakami. S. Nakamura, M. Irie, *Adv. Mater.* **2003**, *15*, 121.

Photonic Band Engineering in Opals by Growth of Si/Ge Multilayer Shells**

By *Florencio García-Santamaría, Marta Ibisate, Isabelle Rodríguez, Francisco Meseguer*, and *Cefe López**

For a number of years the achievement of a structure with a complete photonic bandgap[1] (cPBG) in the optical range has been seen as a major goal in materials science. The numerous promising applications[2] and challenges that are represented by the fabrication of large-scale three-dimensional (3D) crystals justify efforts directed towards this end. Lithography,[3,4] holography,[5] and self-assembly[6] are among the many approaches followed. There are, however, interesting effects that do not rely on the existence of a cPBG, such as the superprism[7] effect or all-angle negative refraction.[8] In this sense, being able to engineer the shape of photonic bands in different frequencies of the spectrum is a desirable aim.

Artificial opals are crystals obtained from self-assembly methods that provide a periodic arrangement of colloidal particles forming a face-centered cubic (fcc) lattice. These structures are often used as matrices to be loaded with semiconductors. If the matrix is etched away, it is called an inverse opal.[9] When the loaded material refractive index is above 2.8 a cPBG can be achieved.[10] Artificial opals present some disadvantages when compared to other structures such as diamond-like opals.[11] The refractive index contrast must be rather large (> 2.8) and the cPBG opens at high energies (between the 8th and 9th bands). This results in a gap severely affected by the presence of defects.[12] Nevertheless, the use of artificial opals as 3D photonic crystals is already well established among researchers in this field. The low cost of fabrication, large domains, and high-quality optical response are their primary advantages.

The potential of Si and Ge as materials for photonic applications has been well established since the appearance of two works published by Blanco et al.[13a] and Míguez et al.[13b] For the first time they presented crystals (based on opals) accomplishing all the requirements to present a cPBG in the near infrared (NIR). Apart from their high refractive indices, both materials have a long established technological tradition. Many efforts have been directed towards the improvement of these crystals[14] and their in-depth study.[15] Self-assembly allows few variations since fcc structures of touching spheres are the most usual result. However, when it comes to band engineering, it must be taken into account that photonic bands not only depend on the underlying lattice but on the primitive cell structure. So, accurate control of the materials composing our fcc crystal is the one remaining tool for band engineering. The use of high refractive index semiconductors importantly affects band structure, and that is what this present work is concerned about. Here we will present a method to accurately control the synthesis of both semiconductors (Si and Ge) within thin silica opals. Simple layers or even multiple layers combining air, Si, and Ge will be presented. By means of this method we will be capable of modifying the photonic properties of our crystals. Optical spectra in excellent accordance to theoretical calculations will be provided to support our results.

To achieve the results presented here, we prepared thin silica opals by vertical deposition[16] on Si substrates. This method is becoming widely used and has increasingly taken over from opals fabricated by sedimentation. A reduced thickness is not a problem since it has been shown that a low number of layers (> 18) may be taken as an infinite crystal.[17] The advantages of vertical deposition are obvious: a shorter preparation time, smaller quantity of spheres, and good control over thick-

[*] Dr. C. López, F. García-Santamaría, M. Ibisate, Dr. I. Rodríguez, Prof. F. Meseguer
Instituto de Ciencia de Materiales de Madrid (CSIC)
Cantoblanco, E-28049 Madrid (Spain)
and
Unidad Asociada UPV-CSIC
Camino de Vera s/n, E-46022 Valencia (Spain)
E-mail: cefe@icmm.csic.es

[**] This work was partially supported by the Spanish CICyT project MAT2000-1670-C04 and the European Commission Project IST-1999-19 009 PHOBOS. FGS thanks T. Leonardo for her valuable editing suggestions.

  DOI: 10.1002/adma.200304866

ness. Also, when loaded with other materials, internal accessibility is higher. However, preparation of these samples is not a well-known matter when silica spheres of diameters above 450 nm are used. This may become a serious problem since larger lattice parameters are needed when opals are host materials for semiconductors such as Si or Ge due to their transparency regions. Currently, there is still a need for a more detailed description of a reproducible procedure. Here we present a route that has been successful to fabricate thin opals from silica spheres of 660 nm diameter. Domains are large enough to obtain good spectra from areas as large as 330 × 330 μm^2. Our method is a modification of previous work[14,16] and must be improved further to control the number of layers and homogeneity. However the samples we produced were ideal for use in the experiments presented here.

Both amorphous semiconductors were synthesized by chemical vapor deposition (CVD) performing slight modifications over already published methods. In the case of Si the precursor gas was disilane (Si_2H_6) and the selected decomposition temperature was 375 °C. For Ge, the precursor was germane (GeH_4) and the decomposition temperature 270 °C. Lower temperatures resulted in very slow synthesis rates while higher ones allowed little degree of control. It was observed that high temperatures induce the growth of undesired particles. Indeed, as Figures 1a,b show, large spherical particles of Si or tubular Ge wires grew on the sample surface.

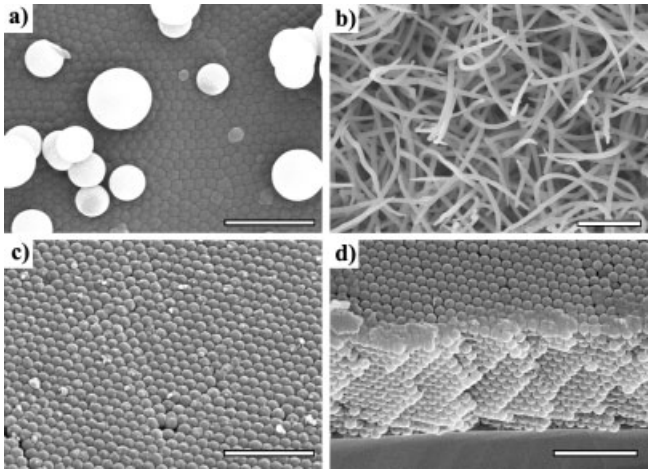

Fig. 1. Top images show unwanted particles in a) silicon (450 °C) and b) germanium (350 °C). This "contamination" is drastically reduced at lower temperatures for c) silicon (375 °C) and d) germanium (270 °C). Opals are made from silica spheres of 660 nm diameter. All scale bars are 5 μm.

Due to their high refractive indices, these particles severely affect the optical measurements making the spectra rather difficult to interpret. The similarity existing between Figure 1b and the α-GeO_2 nanowires recently presented and studied by Hu et al. is, however, noticeable.[18] These samples contrast with the clean surfaces of the resulting composites (Figs. 1c,d) at the optimized temperatures.

To calculate the percentage of semiconductor present in the pores, reflectance spectra of the samples were measured. The spectra were then compared to the band structures. Theoretical calculations[19] were done assuming that semiconductor growth is layered, meaning that silica spheres are surrounded by semiconductor shells.[20] The refractive index values used for SiO_2, Si, and Ge were 1.43,[21] 3.80,[22] and 4.10,[22] respectively.

Figure 2 shows an example of control of degree of infiltration of amorphous Ge. In these spectra we can observe the diffraction peak caused by the first pseudo-gap, the Fabry–

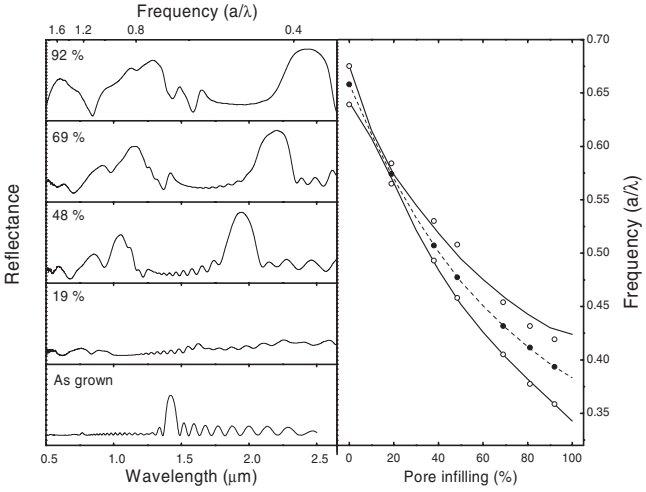

Fig. 2. Left panels show the reflectance spectra of the samples loaded with different amounts of Ge for opals of 660 nm diameter spheres. The right panel shows the center (full circles) and edges (open circles) of the first pseudo-gap in the {111} direction as a function of germanium layer thickness along with the theoretical calculations (lines). Frequency units are normalized to the lattice parameter.

Perot fringes due to the finite thickness of the sample, and other reflection peaks associated with various other photonic bands. Apart from the percentage of loaded semiconductor some other information can be deduced from the spectra. From the Fabry–Perot fringes the thickness of the sample can be extracted. Our thin opals were typically made of 14–16 layers, having a final thickness of 13–15 μm. The right panel in Figure 2 summarizes positions and peak widths of the first pseudo-gap extracted from reflectance spectra as in the left panels. For a low semiconductor filling fraction the full width at half maximum (FWHM) decreases with increasing infiltration and then increases again after further loading. The pseudo-gap almost closes for 15 % Ge in the pores and 20 % in the case of Si (not shown). We shall refer to this percentage as the index matching infilling value (IMIV). This is the result of matching the effective refractive index of the pore (air–semiconductor) and the silica spheres. It is important to mention that the effective refractive index of the pore differs from the average value, the reason being that we are working with a layered model.[20] The FWHM of the experimental Bragg diffraction peaks is compared with theoretical expectations in the right panel of Figure 2. The agreement is fairly good.

Around the first pseudo-gap the wavelength involved is close to the lattice parameter for which reason the sample is viewed as a uniform medium and Fabry–Perot fringes show

ADVANCED MATERIALS

up. (The features of the fringes are determined by the sample thickness and effective refractive index). This is much more so near the IMIV, where any contrast in the system is washed out making the samples behave like a thoroughly homogeneous thin film. Here, the Bragg reflectance peak will be indistinguishable from the rest of the fringes. It is, however, interesting to notice that even at the IMIV the sample's crystalline nature can be probed by shorter wavelengths as seen at higher energies. Indeed, although the spectra show that the first pseudo-gap has almost disappeared, some structure related to the 5th to 9th bands can be observed.

The key parameter to control the amount of semiconductor loaded in the opals is reaction time. Figure 3 summarizes the percentage of pore loaded with Si or Ge as a function of synthesis time. It is important to mention that time lengths are quite reasonable since layer thickness variations of only a few nanometers may be achieved with just a few minutes difference. The inset in Figure 3 shows a numerical calculation plotting the pore infilling ratio as a function of layer thickness (normalized to the lattice constant). Under our experimental conditions, we can see that, for a single reaction, Si reaches a maximum at approximately 53 % pore infilling (24 nm layer thickness for opals made of 660 nm silica spheres). In the case of Ge, the pore can be loaded without saturation. Pressure built up by hydrogen production is a limiting factor since it will inhibit the synthesis of the semiconductor. This factor is more important for Si since there is more gas involved in the reaction; in addition, the temperature for Si is 105 °C higher and, again, involves higher pressure. This is probably the reason for such a saturation curve. The temperature at which Ge is grown is very close to the decomposition temperature of GeH_4. This transformation begins with the formation of GeH_2 species.[23] At such a low temperature, the activation energy needed to complete the first step delays the final reaction as can be observed in Figure 3. Thus Si, as opposed to Ge, will need further cycles to obtain higher filling fractions. The only limitation to complete infilling seems to be a geometrical one related to the closure of the pores in the {111} close packed planes. This happens for a grown layer of thickness equal to 5.47 % of the lattice constant (corresponding to an 86 % infilling).[24] Of course, this top limit is valid for defect-free samples. Polydispersity in sphere diameter and vacancies may lead to this value being exceeded. This explains why filling ratios close to 100 % have been reported.[13,20]

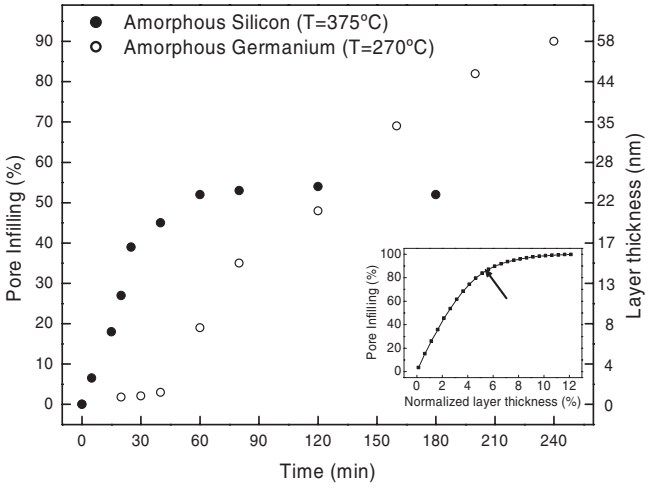

Fig. 3. Infilling as a function of single reaction times. Si (full circles) is formed at 375 °C and Ge (open circles) at 270 °C. Silica spheres of 660 nm diameter are used. The inset shows the semiconductor layer thickness dependence of filling fraction for a fcc lattice. Layer thickness is normalized to lattice parameter. The arrow points at the value where the {111} plane pores are closed.

With this degree of control over the Si and Ge growth we can tackle the growth of multilayer structures. Our method allows not only growth of both materials on silica but either on the other, as will be shown shortly. A further degree of freedom will be provided by the selectivity of different solvents that can be used to remove some of the materials. Aqua regia (a [3:1] mixture of hydrochloric and nitric acid) can selectively remove Ge, damaging neither the silica spheres nor the Si layer. Furthermore, Ge can be oxidized at 500 °C without changing the properties of the rest of the materials: silica spheres remain unaffected[21] and Si requires higher temperatures for its oxidation. All these methods are compatible with the new technique developed by Ozin and co-workers to directly grow silica by CVD at room temperature and atmospheric pressure.[24]

To test the possibility of loading a multilayer of semiconductor, a sample with 30 % of the pore loaded with Ge was re-grown with Si up to 80 %. Then, Ge was etched with aqua regia. Figure 4 shows a electron microscopy image of the resulting structure after etching. The Si network is interconnected and fixed to the substrate and remains separated from the spheres by the air layer.

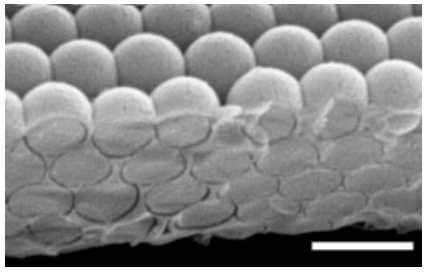

Fig. 4. Cleaved edge scanning electron microscopy (SEM) image of a doubly connected structure. The sample shows the continuous Si layer separated from the continuous silica structure by an air shell. The dark lines in the cleaved edge are the air gaps between Si shell and silica spheres. Scale bar is 1 μm.

A more complicated structure was fabricated and optically characterized. First a sample was loaded with Si up to 20 % of the pore, then a layer of Ge to complete 45 %, and finally Si to 60 % pore infilling. At this point the composite presents the following composition: SiO_2 (74 %), Si (5.2 %), Ge (6.5 %), Si (3.9 %); with the percentages representing the total volume fraction of each material with 10.4 % air remaining. This sample was then dipped in aqua regia for 60 min. The outcome is two homogeneous Si shells separated by an air gap and grown on silica spherical cores.

Figure 5 shows the reflectance spectra evolution at different stages. The bare opal (Fig. 5a) is loaded with Si (Fig. 5b) up to a value close to the IMIV. The first pseudo-gap all but disappears while higher energy features become clearer. Further

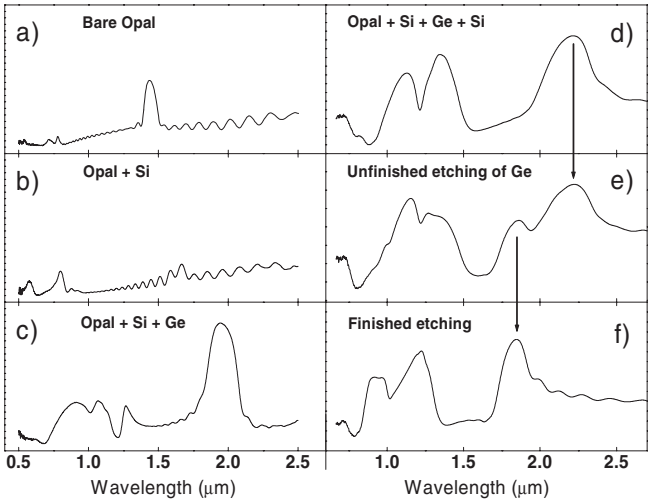

Fig. 5. Reflectance spectra of a sample after successive semiconductor infilling and etching. a) Bare opal; b) a Si layer is grown; c) a second layer of Ge; and d) a third layer of Si are grown; e) partial etching of the Ge; f) etching is completed and regions with a pseudo-gap at 2.22 μm disappear.

loading with Ge (Fig. 5c) raises the first pseudo-gap and increases the width of the reflectance peaks. A new layer of Si (Fig. 5d) further red-shifts and widens the photonic features. At this point, Ge begins to be etched. Before it is completely removed, the spectra collect information from areas with and without Ge. For this reason both peaks corresponding to the first pseudo-gap before and after removing Ge appear in the spectrum (Fig. 5e) at 2.22 μm and 1.85 μm respectively. After 60 min etching was completed (Fig. 5f) and the peak at 2.22 μm had completely disappeared.

Yet another tool is hydrofluoric acid (HF), which can selectively remove both oxides. The following four-step process illustrates a particular case where this technique may be applied to tailor the photonic bands. First, an opal is loaded with Ge to 25 % of the available volume, followed by its oxidation. A further Ge load completes 86 % of the initially available volume. Finally the oxides (GeO_2 and SiO_2) are removed with HF. The corresponding photonic band structure is shown in Figure 6. Two cPBGs open up: a larger one (12.6 %) between the 8th and 9th bands and a narrower one (1.3 %) between the 5th and 6th bands. The latter is an interesting case that was reported only very recently for fcc-based structures.[25]

In summary, controlled growth of amorphous Si and Ge within thin silica opals has been performed. Optical characterization of the samples has shown that accurate control of the amount of semiconductor loaded is feasible. The possibility of fabricating opal structures with a multilayer of alternating air, Si, and Ge has been demonstrated. A whole wealth of techniques is available if we add the selective oxidation and removal of the various compounds synthesized. The calculations

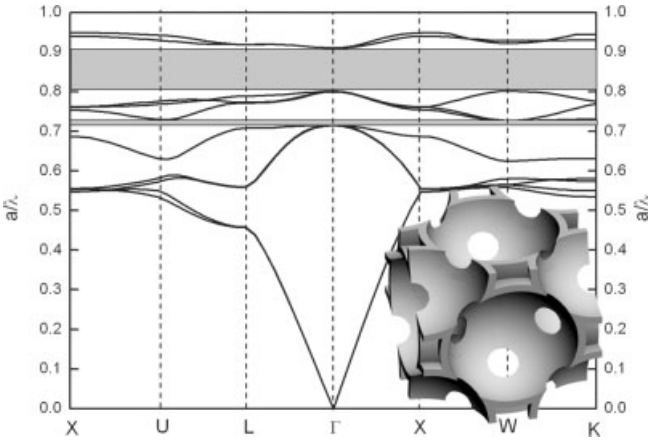

Fig. 6. Photonic band diagram of interpenetrating air spheres coated with amorphous Ge ($n = 4.1$) in a fcc lattice, with $a = 0.3645$ being the radius of the air spheres and $a = 0.4087$ the external radius of the semiconductor shell. Two gaps are developed: one between the 5th and 6th and another between the 8th and 9th bands. The inset shows the corresponding real space structure.

for one structure that can be obtained by this method show a gap between the 5th and 6th bands. This encourages us to perform further calculations to study the formation of this gap or the evolution of high-energy bands at low semiconductor filling ratios.

Experimental

Thin Opal Fabrication: Firstly, silica spheres 660 nm in diameter are synthesized by means of the Stöber–Fink–Bohn [26] method. Although it has been said [16] that a coating of 3-(trimethoxysilyl)propyl methacrylate (TPM) is not a key parameter in film deposition of smaller spheres it is our experience that order in samples is increased when TPM is used. The spheres are then dispersed in ethanol (0.8 vol.-%). Si substrates (6 cm × 2 cm) are carefully cleaned in a solution of HF (1 %) and afterwards another of H_2SO_4/H_2O_2 (2:1 vol/vol). Finally the substrates are rinsed in doubly distilled water, acetone, and ethanol. The dispersion of silica spheres and the substrates are placed in a clean scintillation vial (30 mL) within a furnace at 36 °C and covered with a beaker. It is important not to set the substrates completely vertical (30 to 40 inclination degrees with respect to the vertical direction) or too thin opals (1–3 layers) are obtained.

Chemical Vapor Deposition: The precursor pressure was fixed at 150 torr. It is preferred to higher pressures to increase safety. The procedure to synthesize the semiconductors has been previously reported [13]. Liquid nitrogen is used to condense the precursor gas (disilane or germane) in the cell where synthesis takes place. Of course the whole system is previously subjected to high vacuum (3×10^{-6} torr) to avoid the presence of air. The cell is then placed in a furnace at the optimum temperature.

Optical Characterization: The measurements were performed with a Fourier transform infrared spectrometer (FTIR), IFS 66S from Bruker with a IRScope II microscope attached. A 4× objective with a numerical aperture of 0.10 was used to focus and collect the light. Light was collected at normal incidence with respect to the (111) family of planes.

Received: January 14, 2003
Final version: February 28, 2003

[1] a) E. Yablonovitch, *Phys. Rev. Lett.* **1987**, *58*, 2059. b) S. John, *Phys. Rev. Lett.* **1987**, *58*, 2486.
[2] J. D. Joannopoulos, P. R. Villeneuve, S. Fan, *Nature* **1997**, *386*, 143.
[3] N. Yamamoto, S. Noda, A. Chutinan, *Jpn. J. Appl. Phys.* **1998**, *37*, 1052.
[4] J. G. Fleming, S.-Y. Lin, *Opt. Lett.* **1999**, *24*, 49.
[5] M. Campbell, D. N. Sharp, M. T. Harrison, R. G. Denning, A. J. Turberfield, *Nature* **2000**, *404*, 53.
[6] G. M. Whitesides, B. Grzybowski, *Science* **2002**, *295*, 2418.

ADVANCED MATERIALS

[7] H. Kosaka, T. Kawashima, A. Tomita, M. Notomi, T. Tamamura, T. Sato, S. Kawakami, *Appl. Phys. Lett.* **1999**, *74*, 1370.
[8] C. Luo, S. G. Johnson, J. D. Joannopoulos, J. B. Pendry, *Phys. Rev. B* **2002**, *65*, 201 104–1.
[9] B. T. Holland, C. F. Blanford, A. Stein, *Science* **1998**, *281*, 538.
[10] H. S. Sözüer, J. W. Haus, R. Inguva, *Phys. Rev. B* **1992**, *45*, 13 962.
[11] a) F. García-Santamaría, H. T. Miyazaki, A. Urquía, M. Ibisate, M. Belmonte, N. Shinya, F. Meseguer, C. López, *Adv. Mater.* **2002**, *14*, 1144. b) F. García-Santamaría, C. López, F. Meseguer, F. López-Tejeira, J. Sánchez-Dehesa, H. T. Miyazaki, *Appl. Phys. Lett.* **2001**, *79*, 2309.
[12] M. M. Sigalas, C. M. Sokoulis, C. T. Chan, R. Biswas, K. M. Ho, *Phys. Rev. B* **1999**, *59*, 12 767.
[13] a) A. Blanco, E. Chomski, S. Grabtchak, M. Ibisate, S. John, S. W. Leonard, C. López, F. Meseguer, H. Míguez, J. P. Mondía, G. A. Ozin, O. Toader, H. M. van Driel, *Nature* **2000**, *405*, 437. b) H. Míguez, E. Chomski, F. García-Santamaría, M. Ibisate, S. John, C. López, F. Meseguer, J. P. Mondía, G. A. Ozin, O. Toader, H. M. van Driel, *Adv. Mater.* **2001**, *13*, 1634.
[14] Y. A. Vlasov, X.-Z. Bo, J. C. Sturm, D. J. Norris, *Nature* **2001**, *414*, 289.
[15] E. Palacios-Lidon, A. Blanco, M. Ibisate, F. Meseguer, C. López, J. Sánchez-Dehesa, *Appl. Phys. Lett.* **2002**, *81*, 4925.
[16] P. Jiang, J. F. Bertone, K. S. Hwang, V. L. Colvin, *Chem. Mater.* **1999**, *11*, 2132.
[17] J. F. Bertone, P. Jiang, K. S. Hwang, D. M. Mittleman, V. L. Colvin, *Phys. Rev. Lett.* **1999**, *83*, 300.
[18] J.-Q. Hu, Q. Li, X-M. Meng, C.-S. Lee, S-T. Lee, *Adv. Mater.* **2002**, *14*, 1396.
[19] The eigenstates are computed using a plane wave basis in an iterative implementation as described in S. G. Johnson, J. D. Joannopoulos, *Opt. Express* **2001**, *8*, 173. MIT Photonics-Bands (MPB) package v-013.
[20] A. Blanco, H. Míguez, F. Meseguer, C. López, F. López-Tejeira, J. Sánchez-Dehesa, *Appl. Phys. Lett.* **2001**, *78*, 3181.
[21] F. García-Santamaría, H. Míguez, M. Ibisate, F. Meseguer, C. López, *Langmuir* **2002**, *18,* 1942.
[22] *Landolt-Bornstein: Numerical Data and Functional Relationships in Science and Technology*, Vol. III/17 a (Ed: O. Madelung), Springer, Berlin **1982**.
[23] S. D. Chambreau, J. Zhang, *Chem. Phys. Lett.* **2002**, *351*, 171.
[24] H. Míguez, N. Tétreault, B. Hatton, S.-M. Yang, D. Perovic, G. A. Ozin, *Chem. Commun.* **2002**, *22*, 2736.
[25] W. Dong, H. Bongard, B. Tesche, F. Marlow, *Adv. Mater.* **2002**, *14*, 1547.
[26] W. Stöber, A. Fink, E. Bohn, *J. Colloid Interface Sci.* **1968**, *26*, 62.

Large-Diameter Single-Walled Carbon Nanotubes Synthesized by Chemical Vapor Deposition**

By *Quan-Hong Yang*, *Shuo Bai*, *Jean-Louis Sauvajol*, and *Jin-Bo Bai**

The diameter and helicity are believed to be the parameters that control the unusual physical, mechanical, and chemical properties of single-walled carbon nanotubes (SWNTs). However, it is difficult to experimentally confirm these predictions systematically. SWNTs with a most-frequent diameter of 1.4 nm can be grown by the usual laser vaporization method[1] and the electric arc method.[2] Cheng et al. obtained SWNTs with a mean diameter of 1.69 ± 0.34 nm through a catalytic hydrocarbon decomposition.[3,4] Liu et al. prepared SWNTs with a mean diameter of 1.72 ± 0.2 nm by a hydrogen electric arc method.[5] Kiang synthesized SWNTs with an average diameter of around 2.0 nm by a modified electric arc method.[6] In Cheng and Kiang's samples, a few large SWNTs (Cheng: 4.3 nm, Kiang: 7.0 nm) were noticed. Recently, Lebedkin et al. used laser vaporization to prepare SWNTs approaching 6 nm diameter but with a large dispersion in diameter.[7] Raman spectra showed the abundant existence of small-diameter SWNTs. Generally, one can control the growth process of small-diameter SWNTs to some extent, however, not yet the selective growth of large-diameter SWNTs.

In this communication, we report large-diameter (2–5.2 nm) freestanding SWNTs with average diameters greater than 3 nm prepared by chemical vapor deposition (CVD). Scanning electron microscopy (SEM), high-resolution transmission electron microscopy (HRTEM), and Raman spectrum analyses were conducted to characterize the obtained products.

Like the common CVD SWNT samples,[3,4] our samples exist as macroscopic ropes several centimeters in length. SEM observations (Figs. 1A and B) show that the as-prepared freestanding samples have a preferential orientation and good purity but contain a small amount of amorphous carbon.

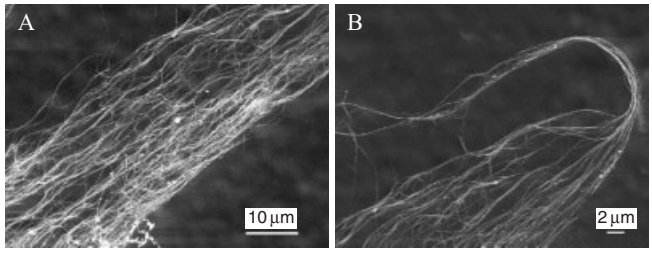

Fig. 1. SEM images of as-prepared large-diameter SWNTs.

Figures 2A–C show typical HRTEM images of our samples composed of SWNTs with large diameter (greater than 2 nm, the isolated SWNT denoted by (c) up to 4.5 nm). Figure 2B shows a small bundle (denoted by (a) in Fig. 2A). The diameters of the four nanotubes in the bundle are 3.4, 3.2, 3.3, and 2.8 nm. Figure 2C shows the cross-sectional images of two bundles with nanotubes of diameter 2.2–2.7 nm, one of which contains tens of nanotubes, and the other, six nanotubes. The diameter distribution histogram of 65 SWNTs, between 2.0 and 5.2 nm, is shown in Figure 3, based on HRTEM images similar to those in Figure 2. Of the 65 SWNTs, 70% of them lie in the range 2.4–4.0 nm, the Gaussian mean diameter being 3.23 ± 0.11 nm. It should be noted that small-diameter (≤ 2.0 nm) nanotubes were rarely observed in these samples. The average diameter is larger than those reported by other authors.[1–7]

Large-diameter nanotubes appear to be more stable, as predicted by the energetic argument that the strain energy per carbon varies with radius R as $1/R^2$.[8] However, the bundles

[*] Dr. J.-B. Bai, Dr. S. Bai,[+] Dr. Q.-H. Yang
Laboratoire MSS/MAT, CNRS UMR 8579, Ecole Centrale Paris
F-92295 Chatenay Malabry (France)
E-mail: baijinbo@mssmat.ecp.fr
Dr. J.-L.Sauvajol
GDPC, CNRS UMR 5581, Université Montpellier II
F-34095 Montpellier (France)
[+] On leave from Shenyang National Laboratory for Materials Science, Institute of Metals Research, CAS, 72, Wenhua Road, Shenyang 100016, People's Republic of China.

[**] The postdoctoral fellowship of QHY was provided by the French Ministry of Research, and that of SB was provided by the French Embassy in Beijing.

  DOI: 10.1002/adma.200304567